Supporting Information for

Correlative Cryogenic Spectromicroscopy to Investigate

Selenium Bioreduction Products

Sirine C. Fakra[*,†,§], Birgit Luef[†,⊥], Cindy J. Castelle[†], Sean W. Mullin[†,#], Kenneth H. Williams[‖], Matthew A. Marcus[§], Denise Schichnes[‡], and Jillian F. Banfield[†,‖]

[†]*Department of Earth and Planetary Science and* [‡]*Department of Plant & Microbial Biology, University of California Berkeley, Berkeley, CA 94720, USA.*

[§]*Advanced Light Source and* [‖]*Earth Sciences Division, Lawrence Berkeley National Lab, Berkeley, CA 94720, USA.*

[*]Corresponding author: sfakra@lbl.gov, ph: 510-495-2855, fax: 510-486-4102

Present addresses: [⊥]Department of Biotechnology, Norwegian University of Science and Technology, Trondheim 7491, Norway. [#]Division of Geological and Planetary Sciences, California Institute of Technology, Pasadena, CA 91125.

This PDF file includes (24 pages, 12 figures, 4 tables, 2 movies):

- Materials and Methods and Supplementary text
- Figures S1 to S12
- Captions for Movies S1 and S2
- Tables S1 to S4
- References

Other Supplementary Material for this manuscript: Movies S1 & S2 and SeK_standards.zip.

Materials and Methods

Groundwater geochemical measurements. Groundwater samples were collected at a depth of 5m below ground surface in the monitoring well, filtered through 0.45 μm Polyvinylidine Fluoride (PVDF) syringe filters (Merck Millipore, Ireland), acidified to a pH<2 with trace metals grade nitric acid, and analyzed for total selenium concentrations via inductively coupled plasma mass spectroscopy (ICP-MS; Elan DRCII, Perkin−Elmer, CA). Acetate and bromide were measured with a Dionex ICS-2100 chromatograph with a Dionex AS-18 column (Thermofisher Scientific, USA).

Cryo-plunging of samples for synchrotron and TEM analyses. Field-derived biofilm and enrichment culture samples were flash-frozen directly in the field or in the laboratory, respectively. Samples were either mounted on TEM Cu-grids (200 mesh, lacey carbon coated formvar, Ted Pella Inc.) or on Si_3N_4 windows (TEM windows, SiMPore Inc.). TEM grids and Si_3N_4 windows were pre-treated by glow-discharge to improve sample deposition, and were pre-loaded with colloidal gold particles (10 nm, BBInternational, Cardiff, UK) serving as fiducials. Aliquots of 5 μL of fresh biofilm sample solution were deposited onto the grids. The grids were then manually blotted with filter paper (Grade 1 filter paper, Whatman®) and plunged into liquid ethane at LN_2 temperature, using a portable cryo-plunger. All samples were placed in grid boxes and stored in a LN_2 tank until analysis. Further details on the cryo-plunger instrument and procedures can be found elsewhere[1].

Selenium valence state scatter plot. We used a method similar in concept to that described in Marcus et al.[2] (for Fe species) to evaluate the valence state of Se. Normalized XANES spectra

were processed using a new custom Matlab program. Spectra were reduced to two variables, a and b, defined as the normalized XANES absorption values at 12664.25 eV and 12667.80 eV respectively. These energies were determined empirically to lead to the best separation between chemical families in (a,b) scatter plots. Selenate Se(VI), selenite Se(IV), elemental Se(0) and Se(-II) selenide/Se(-I)/Organic Se families are found to clearly separate, as evidenced with Se standards of known valence, plotted in black (**Fig. S9**). Using this method, unknown experimental XANES data could be at first sight classified according to valence state. Least square linear combination fitting is still required to confirm the identity and valence state of the unknown. All standards (see **Table S2**), were recorded at ALS beamline 10.3.2 either at room temperature, with samples mounted on kapton tape, or at 95 K using the cryo-stage, described in the main text, with samples mounted on Si_3N_4 windows (TEM windows, SiMPore Inc.).

Micro-X-ray diffraction. Data were collected in transmission with a CCD camera (Bruker SMART6000) at 17 keV ($\lambda = 0.729$ Å) using a beam spot size of 12×7 μm and exposure times of 240 sec. A background pattern was also recorded nearby the region of interest. Calibration of the camera distance was obtained using an alumina (α-Al_2O_3) powder standard and Fit2D software[3]. Fit2D was also used to obtain one-dimensional XRD profiles from the radial integration of 2D patterns. XRD peaks were indexed using Jade 9 software (Materials Data Inc.) and the ICDD PDF-4+ database. Additional cards from Mincryst for red monoclinic Se^0, grey trigonal-Se^0 and hexagonal ice were added to the database.

Confocal laser scanning microscopy (CLSM). CLSM was performed on a cross section of the tubing with biofilms attached on the inner surface. Samples were fixed in 2.5 % Paraformaldehyde (final concentration). Confocal images were acquired on a Carl Zeiss Inc. LSM 710 Zen 2010

Black (Carl Zeiss MicroImaging Inc., Thornwood, NY, USA), equipped with an Argon 488 nm laser. A 63x CPlanApo water immersion objective was used to acquire z-stack images at 1024x1024, 8 bit resolution. The pinhole was set to 1 Airy unit, yielding an optical slice thickness of 0.8 um. The step size was set to Nyquist sampling, at 0.4 um. Samples were stained with SYTO BC (Invitrogen product #S34855) and mounted in water in a glass depression slide with a coverslip measuring 173 um in thickness. All 3-D renderings were performed using Imaris software (Bitplane AG, Zurich, Switzerland).

16S ribosomal RNA gene sequencing. DNA was extracted from biofilm samples using the PowerSoil DNA Extraction Kit (MoBio Laboratories, Inc., CA, USA) according to specifications of the manufacturer, except that the initial lysing step was accomplished by vortexing at maximum speed for 2 minutes and then incubating at 65 °C for 30 minutes, with an additional minute of vortexing every 10 minutes. DNA was amplified using 27f and 1492r primers over a temperature gradient, and PCR products were cleaned up using the MoBio UltraClean PCR Clean-Up Kit. The amplified DNA was then used to create 16S rRNA gene clone libraries with the pCR 2.1-TOPO vector according to manufacturer specifications and electrocompetent cells. Generated sequences from successful insertions were trimmed to remove Phred quality scores ≤20, with forward and reverse sequences assembled via Phrap. Each sequence was then BLASTed against the SILVA SSURef108 database.

16S rRNA gene phylogenetic analysis. 16S rRNA gene sequences were aligned using SSU-Align[4] along with the best-hits of these sequences in the SILVA database (version 115 of non-redundant SILVA)[5], a curated set of reference bacterial sequences, and a set of archaea sequences **(Fig. 3B).** A set of Gammaproteobacteria **(Fig. 3C and 3D)** served as a phylogenetic root.

Sequences with ≥800 bp aligned were used to infer a maximum-likelihood phylogeny using RAxML[6] with the GTRCAT model of evolution (**Fig. S4A**), and to construct neighbor-joining trees[7] (**Fig. S4B and S4C**). Bootstrap analyses were based on 100 re-samplings.

Scanning Transmission X-ray Microscopy (STXM). STXM measurements were performed on the soft X-ray beamline 11.0.2 (150-2000 eV) of the Advanced Light Source, Lawrence Berkeley National Lab, Berkeley, CA[8]. This microscope employs a Fresnel zone plate lens (25 nm outer zones) to focus a monochromatic beam onto the sample. The sample is scanned in 2 dimensions through the fixed beam and transmitted photons are detected with a phosphor scintillator-photomultiplier assembly. Image contrast relies on core electron excitation by X-ray absorption[9, 10]. X-ray images recorded at energies just below and at the elemental absorption edge of interest (Se L_3 and C K) were converted into optical density (OD) images and used to derive elemental maps (OD = ln (I_0/I), where I_0 is the incident X-ray intensity and I is the transmitted beam intensity through the sample). Chemical maps were obtained by taking the difference of OD images at 280, 288.2 eV (proteins); 289, 290.3 eV (carbonates); and 1425, 1440 eV (Se). Image sequences ('stacks') recorded at energies spanning the Se $L_{2,3}$-edges (1420-1520 eV) and C K-edge (280-320 eV) were used to obtain XANES spectra from regions of interest. Fitting of the stacks were performed using the stack fit option in aXis 2000 and relevant standards. Se $L_{2,3}$-edges XANES is sensitive to the oxidation state and the local bonding environment of Se. Se spectra were compared to model compounds (see **Table S2,** asterix annotation). The main Se L_3 resonance of the amorphous red Se^0 standard was set to 1435 eV and used for relative energy calibration of the spectra. At least two different sample regions were analyzed for each element. The theoretical spectral and spatial resolutions during measurements were +/-100 meV and 30 nm respectively.

The photon energy was calibrated at the C K-edge using the Rydberg transition of gaseous CO_2 at 292.74 eV (C 1s→ 3s ($v = 0$)). All measurements were performed at ambient temperature under He at pressure < 1 atm. All data were processed with the IDL-based aXis2000 software package (http://unicorn.mcmaster.ca/aXis2000.html). This STXM did not have cryogenic capabilities and flash-frozen samples were thawed and air-dried at room temperature just prior to measurements.

SEM/ EDS. Scanning electron microscopy and energy dispersive spectroscopy data were collected at 5 keV, 15 and 20 keV using an FEI/Philips XL 30 FEG-SEM, equipped with an EDX spectrometer (EDAX, Inc). The specimens were tilted 4 degrees toward the X-ray detector to optimize the X-ray detection geometry. Working distance varied between 7.5 and 10 mm. Collection time for EDS was 500 seconds for each area. The lateral resolution of the microscope was 10 nm at 15 kV.

Supplementary text

X-ray radiation dose rate estimate. We define the dose rate as:

$DR = E/ph \ \times e \times FD \times \mu/\rho$ where:

E/ph= energy (eV) per photon with E = 13 keV and $e = 1.6 \times 10^{-19}$ J

$$FD = Flux\ density = \frac{full\ flux}{full\ spot\ size} = \frac{10^9}{15 \times 6 \times 10^{-12}} = 1.11\ 10^{19}\ ph\ s^{-1}m^{-2}$$

$\mu/\rho = mass\ attenuation\ coefficient \sim 3.5\ cm^2\ g^{-1}\ for\ liquid\ water\ at\ 13\ keV$

Hence, $DR = 8.08 \times 10^3\ J\ kg^{-1}\ s^{-1} = 8.08\ 10^3$ Gy s^{-1}

Micro-XRF mapping used dwell times of 50 ms/pixel typically, hence an X-ray dose on each pixel of ~10^3 Gy. By comparison, Pereiro-López et al.[11] have estimated the critical radiation dose required to image frozen hydrated biological material to be ~10^9 Gy while Fayard et al.[12] have shown that LN_2 cooled blood cells exposed to X-ray doses up to ~ 10^{10} Gy remained well preserved, free of easily visible structural changes and mass loss.
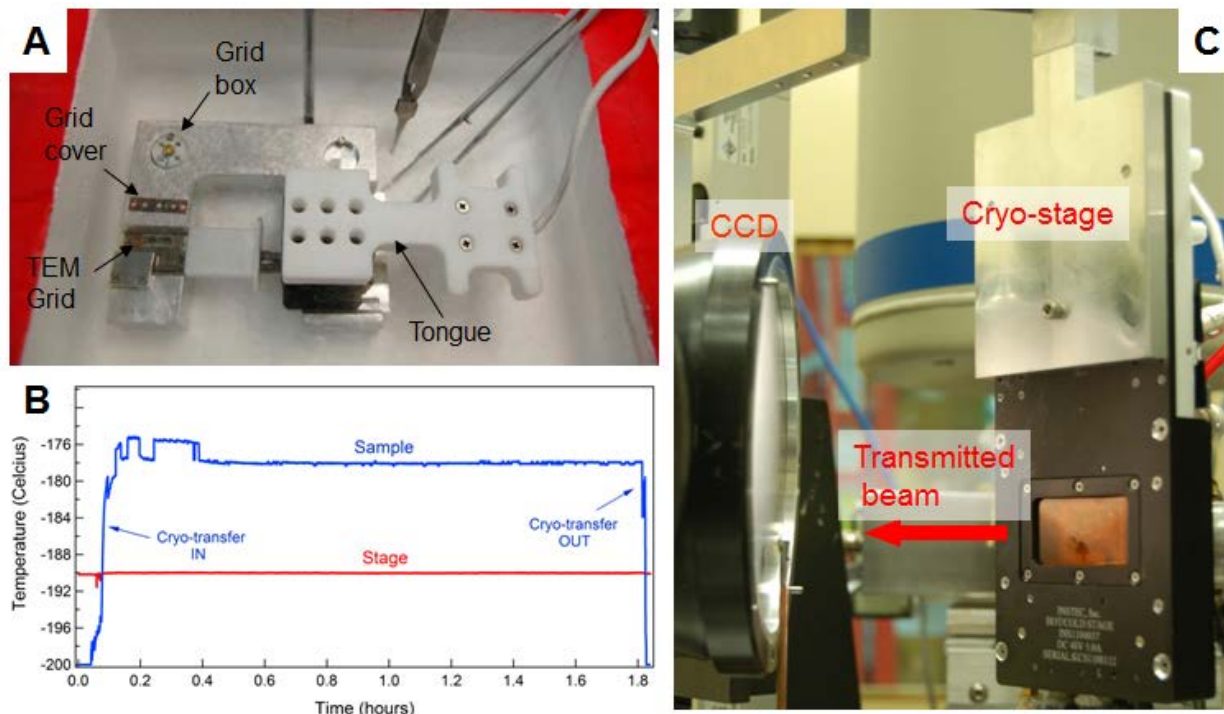
Figure S1. A) Front (beam) view of the sample cryo-transfer tongue accommodating 3 cryo-TEM grids (or Si_3N_4 windows) B) Temperature profiles of the cryo-stage and of the frozen hydrated sample prior, during and after microprobe measurements, showing the evolution of temperature during the transfer of the frozen sample and subsequent measurements once the temperature reaches equilibrium. C) Backside view of the stage, oriented at 45° to incident beam with the sample on the rotation axis and in focus position (regular configuration). Micro-XRD is performed in transmission mode and is used to check the quality of the cryotransfer.
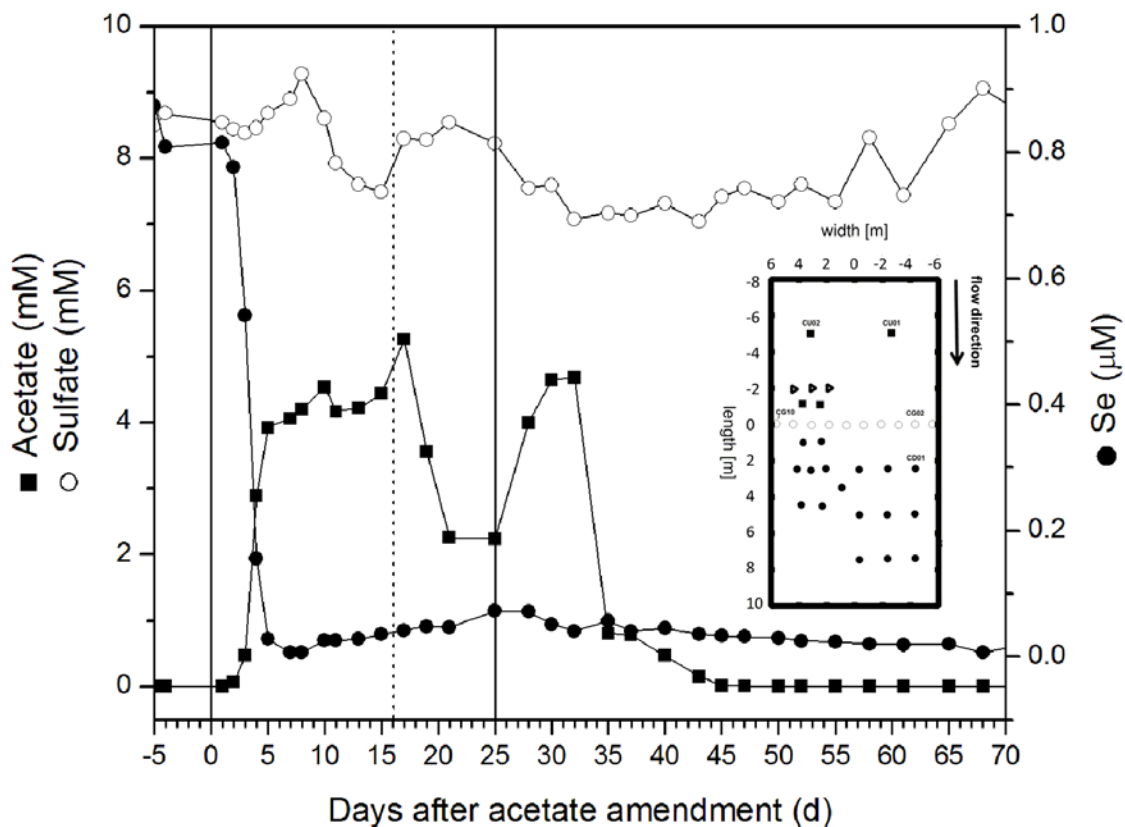
Figure S2. Concentrations of soluble Se, acetate, and sulfate as a function of time in reference well CD01 during the Super 8 experiment at the Rifle site. Solid vertical lines indicate the start and end of acetate injection into the subsurface. Biofilm samples were collected 16 days after the start of acetate amendment (vertical dash line). The decrease in acetate concentration between days 18 and 24 is related to a 6-day gap between two periods of acetate injection. Inset: Location of the down-gradient monitoring well CD01 and acetate injection well CG02 where the biofilms were collected. Further details on the well layout and the Super 8 experiment can be found elsewhere[13].
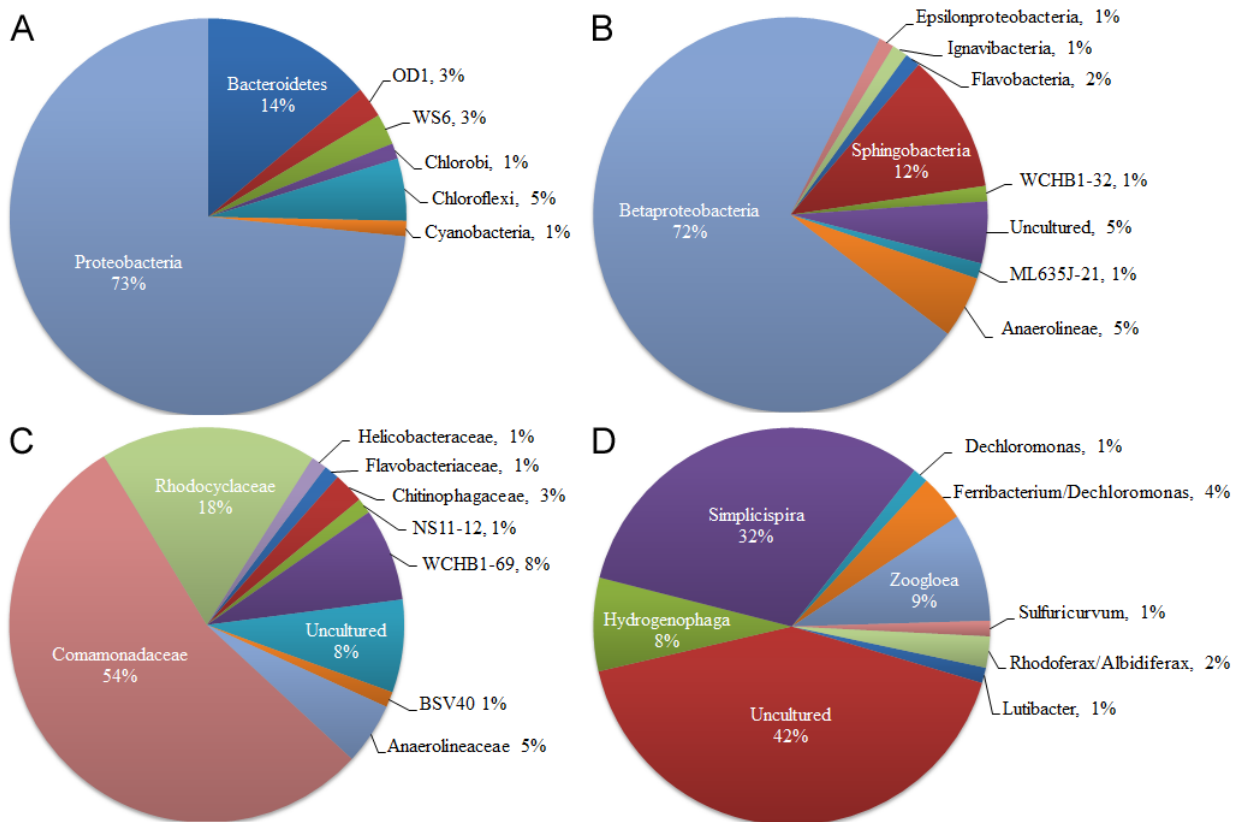
Figure S3. Relative abundance within the Rifle CG02 biofilm microbial community at the A) Phyllum- B) Class- C) Family- and D) Genus-levels. The number of sequences affiliated with each group was divided by the total number of sequences (OTUs).
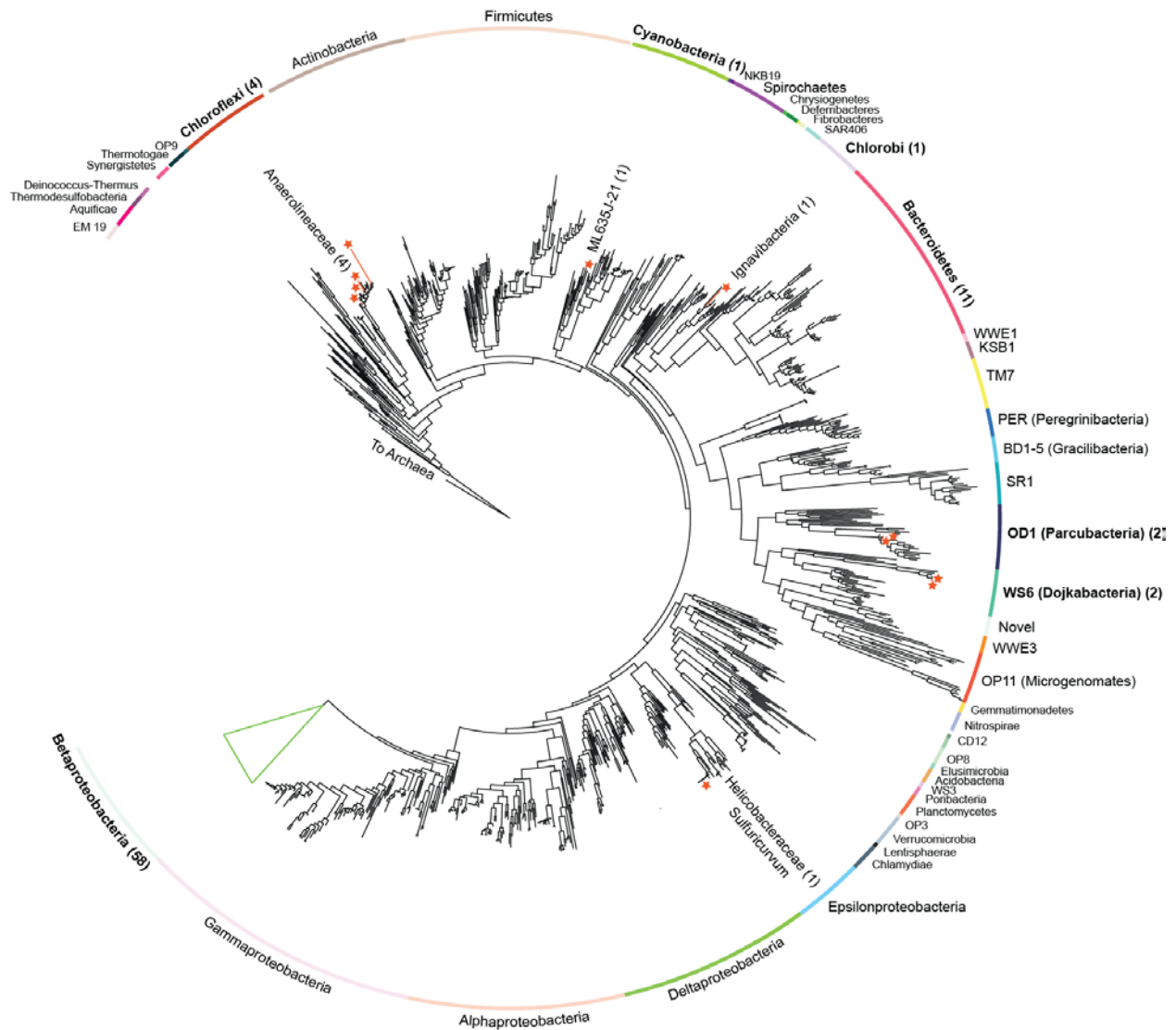
Figure S4A. Maximum-likelihood 16S rRNA gene phylogenic tree. Sequences with ≥800 bp aligned were used to infer a maximum-likelihood phylogeny using RAxML with the GTRCAT model of evolution and 100 bootstrap re-samplings. Red stars represent the 16S rRNA sequences recovered in this study.

Figure S4B. Neighbor-joining tree based on 182 16S rRNA gene sequences showing the phylogenic relationships of the organisms from the Comamonadaceae family sampled in this study (colored in red). Bootstrap values (percentages of 100 replicates) are given at nodes; only values >50% are shown. Gammaproteobacteria were used as an outgroup.
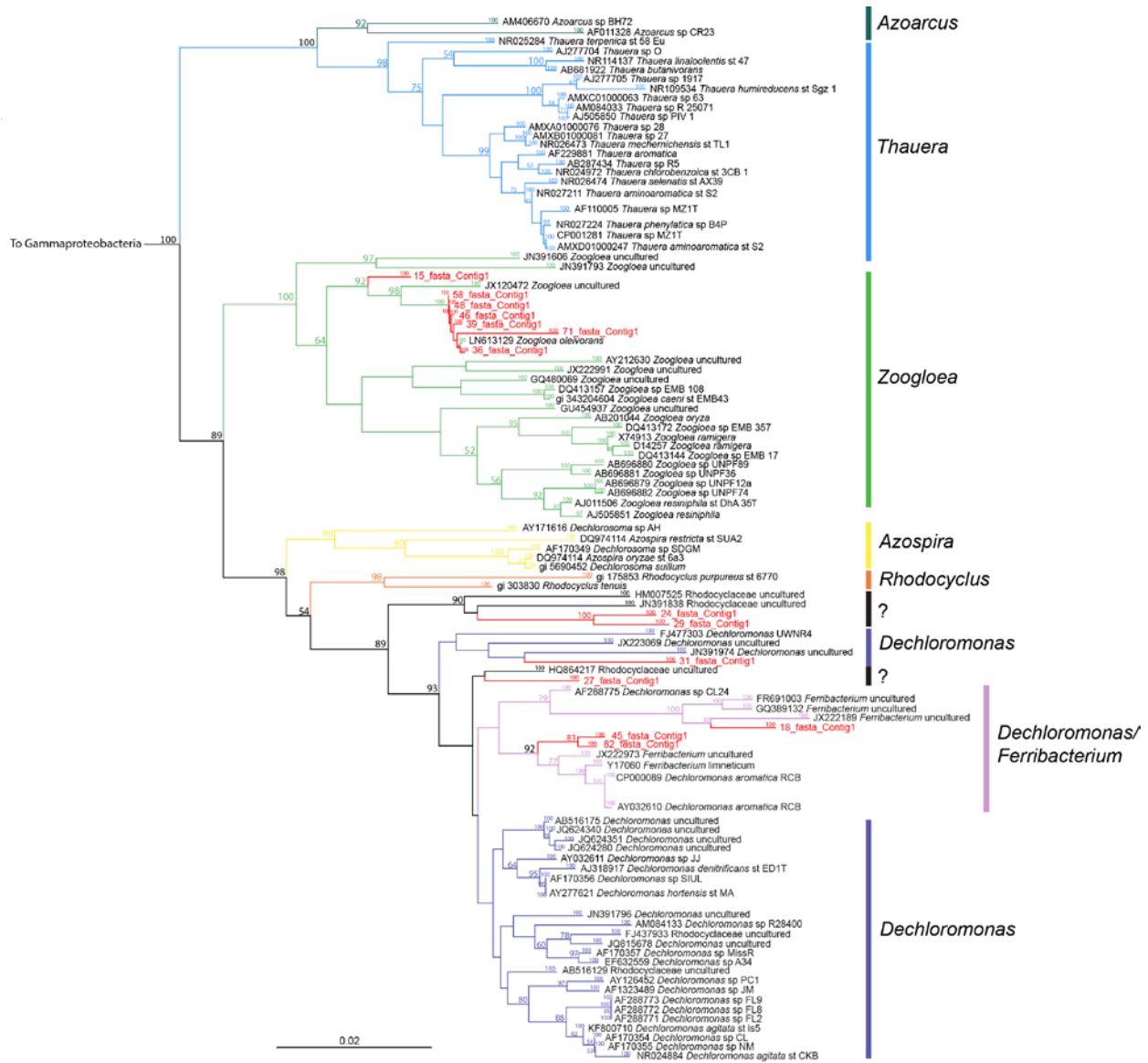
Figure S4C. Neighbor-joining tree based on 111 16S rRNA gene sequences showing the phylogenetic relationships of the organisms from the Rhodocyclaceae family sampled in this study (colored in red). Bootstrap values (percentages of 100 replicates) are given at nodes; only values >50% are shown. Gammaproteobacteria were used as an outgroup.
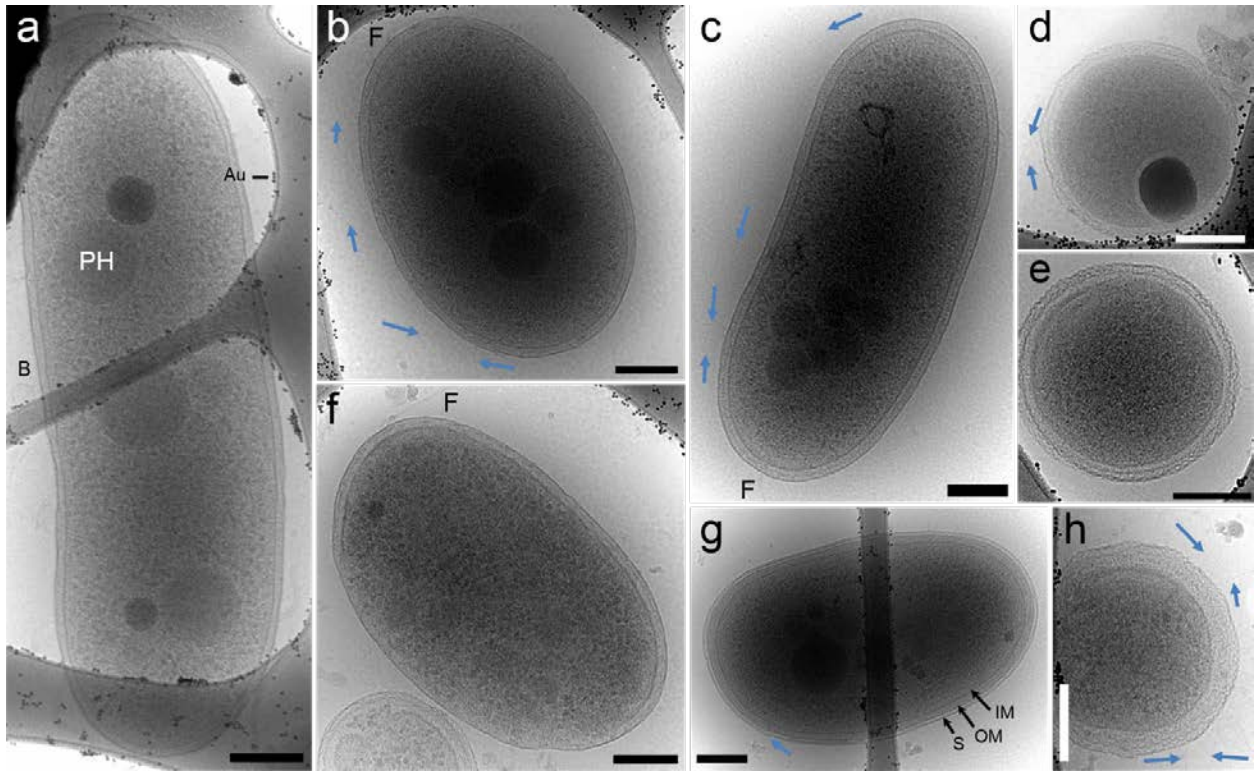
Figure S5. Cryogenic transmission electron micrographs of representative organisms present in biofilm CG02 with approximate dimensions A) 2 µm x 0.63 µm, B) 1.1 µm x 0.78 µm, C) 1.6 µm x 0.65 µm, D) 570 nm diameter, E) 570 nm diameter, F) 1.2 µm x 0.75 µm, G) 1.3 µm x 0.8 µm, H) 550 nm diameter. Most cells contain granules, some have a visible polar flagellum (A, B, E, G), a distinct S-layer (G, D, E, H). Most of them exhibit electron dense particles. Numerous thin pili-like structures (~ 3-6 nm diameter) are found and pointed by blue arrows. F= flagellum, OM= outer membrane, IM= inner membrane, S= S-layer. B= bacteriophage. Au= gold fiducial nanoparticles (10 nm). Scale bars are 200 nm.
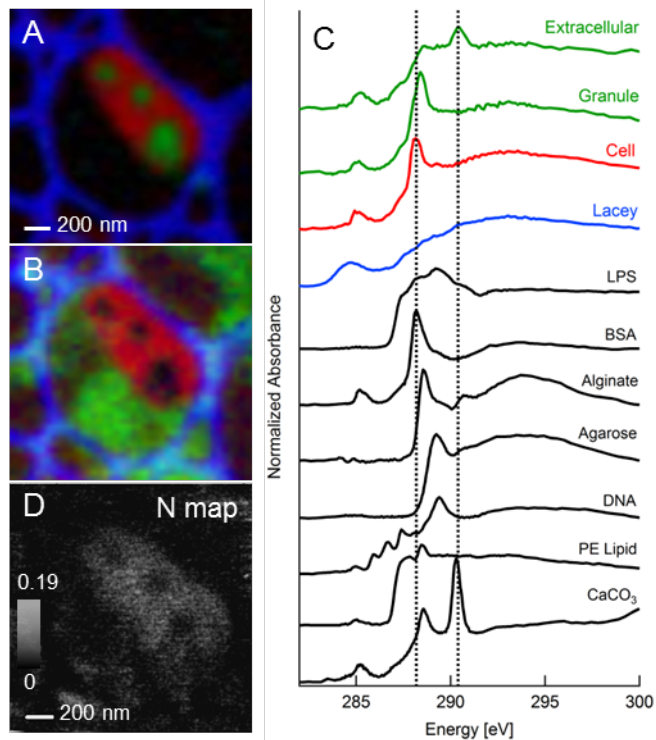
Figure S6. STXM C K-edge data on biofilm CG02. **A)** Tricolor-coded map showing granules (green) inside a cell (red). **B)** Tricolor-coded map of the same region showing extracellular polymeric substances (EPS) in green and cell (granule-free region) in red. The lacey grid is coded in blue in (A, B). Maps were generated by fitting the carbon image sequence ("stack", see methods). **C)** C K-edge XANES spectra of the cell (proteins, 288.2 eV), granules (carboxyls/esters, 288.4 eV) and extracellular substances (acidic polysaccharides, 288.6 and carbonates, 290.3 eV). Standards shown for comparison are: calcite ($CaCO_3$), Lipopolysaccharides from Escherichia coli EH100 (LPS), 1,2-Dipalmitoyl-sn-glycero-3-phosphoethanolamine (PE lipid), bovine serum albumin (BSA) protein, alginate (acidic polysaccharide), agarose (neutral polysaccharide), and DNA standards. All spectra were normalized at 300 eV. Indicative dash lines are at 288.2 eV and 290.3 eV. D) Corresponding nitrogen map shows that the granules are nitrogen-poor.
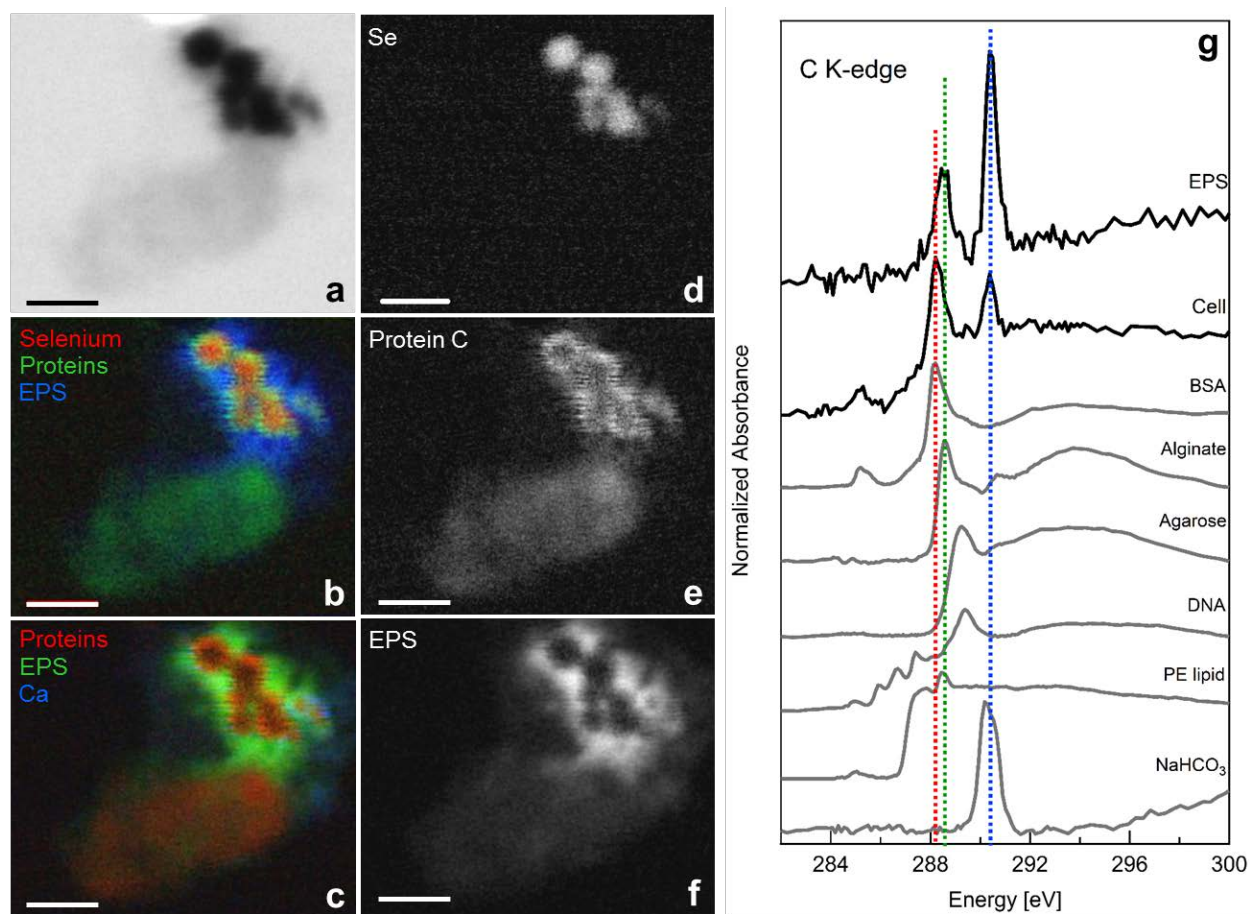
Figure S7. STXM measurements of a 50-day-old culture grown in GWA medium. **a)** Absorption image at 280 eV of a cell and associated Se^0 CNPs. **b-c)** Tricolor-coded maps showing the CNPs coated with proteins, surrounded by extracellular polymeric substances (EPS). Distribution maps of **(d)** Se, **(e)** proteins and **(f)** EPS rich in carbonates and acidic polysaccharides. **g)** C K-edge XANES spectrum of the cell and EPS compared with standards: sodium bicarbonate ($NaHCO_3$, present in GWA medium). Other standards are described in **Figure S6**. All spectra were normalized at 300 eV. Indicative vertical dash lines are at 288.2 (proteins), 288.6 (acidic polysaccharides) and 290.3 eV (carbonates). Scale bars (**a-f**) are 500 nm.
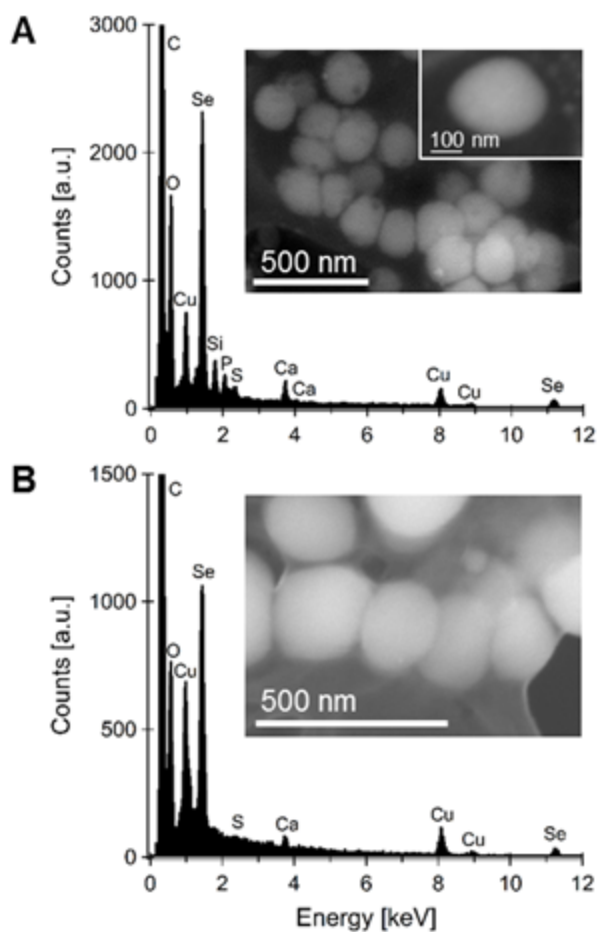
Figure S8. Scanning electron microscopy and energy dispersive spectroscopy of Se^0 CNPs in A) biofilm CG02 and B) a 19-days-old bicarbonate culture. The EDS spectrum shown in (A) was recorded at 15 keV in the small inset area (single particle). The EDS spectrum shown in (B) was recorded at 20 keV in area shown in inset. Cu fluorescence emission peaks were associated with the Cu grid and the C and O peaks originated from the biofilm matrix and the formvar on the grid.
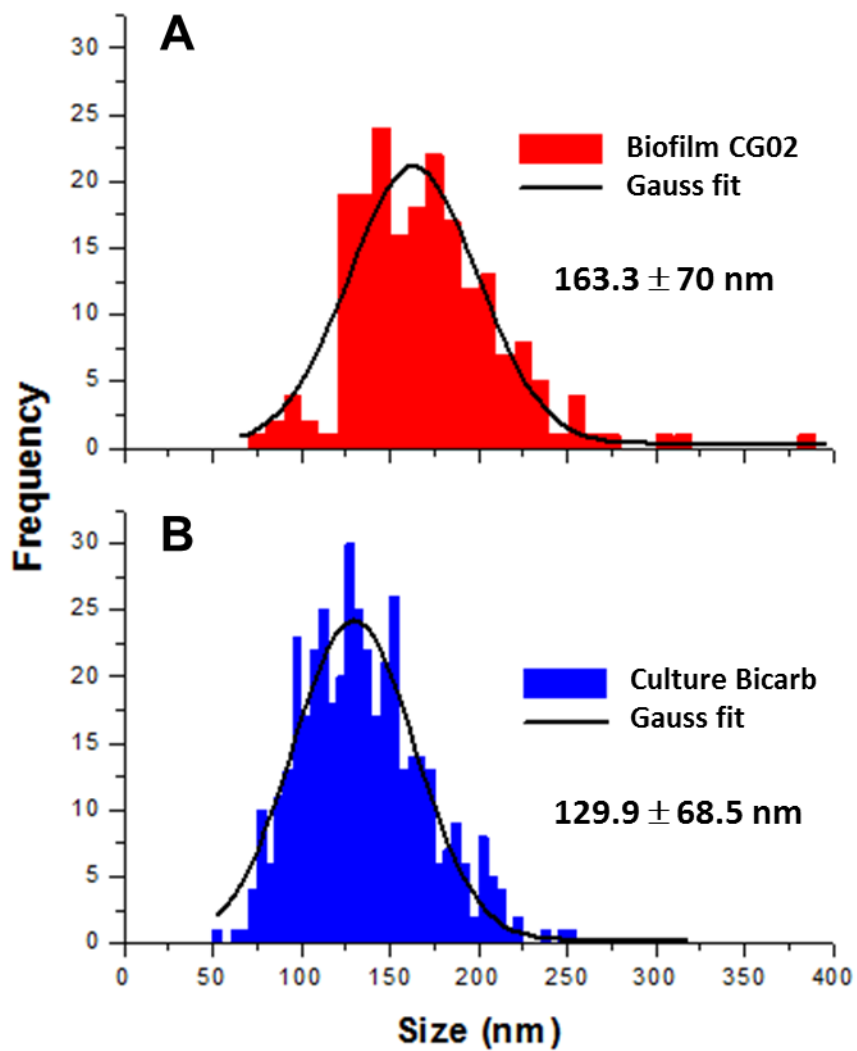
Figure S9. Size distribution of CNPs in A) biofilm CG02 and B) bicarbonate cultures (19-days-old). A total of 199 and 422 particles were respectively measured for (A) and (B), from SEM and TEM images. Gaussian fits of the distributions are also shown.
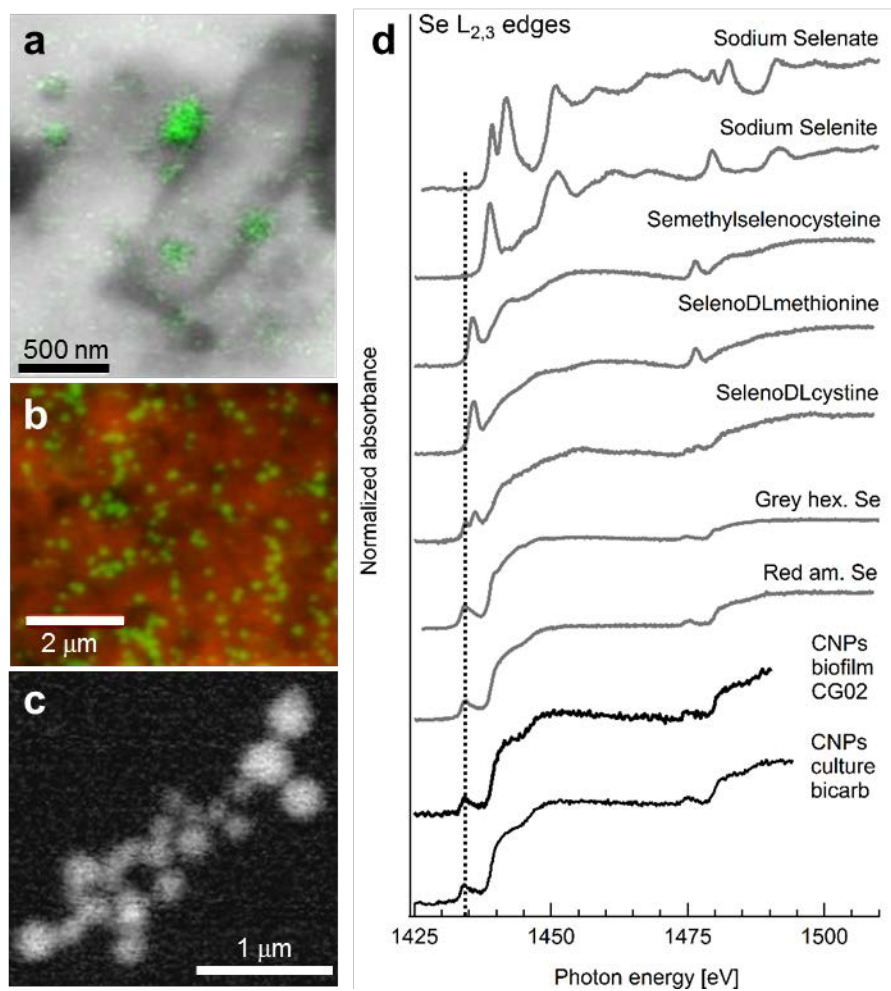
Figure S10: STXM measurements on biofilm CG02: A) Carbon (in red) and selenium (in green) bicolor-coded distribution map. B) Se map (in green) overlaid with an absorption contrast image at 280 eV. C) Se $L_{2,3}$ XANES spectra of Se colloidal nanoparticles (CNPs) compared to Se^0, organic Se, Se(IV) and Se(VI) standards. Abundant extracellular Se^0 CNPs are trapped within the thick biofilm, only few Se CNPs are found associated with each individual cell.
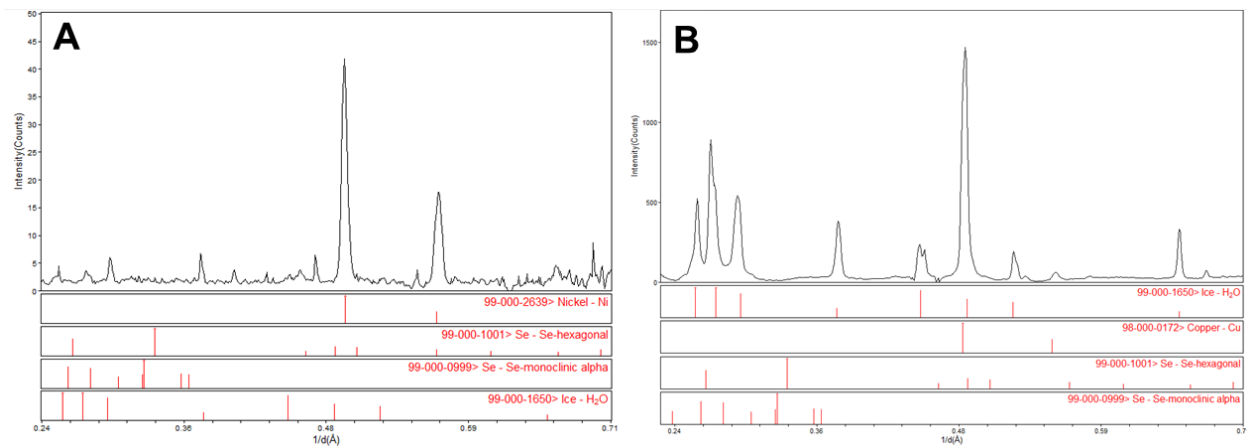
Figure S11: µXRD profiles at 95K of A) the biofilm CG02 and of B) a 19 days-old bicarbonate culture (see the corresponding XRD pattern in **Figure 5**). Both show no evidence for crystalline Se^0, either hexagonal or monoclinic. Cu and Ni peaks are associated with the Cu and Ni-finder grids respectively.
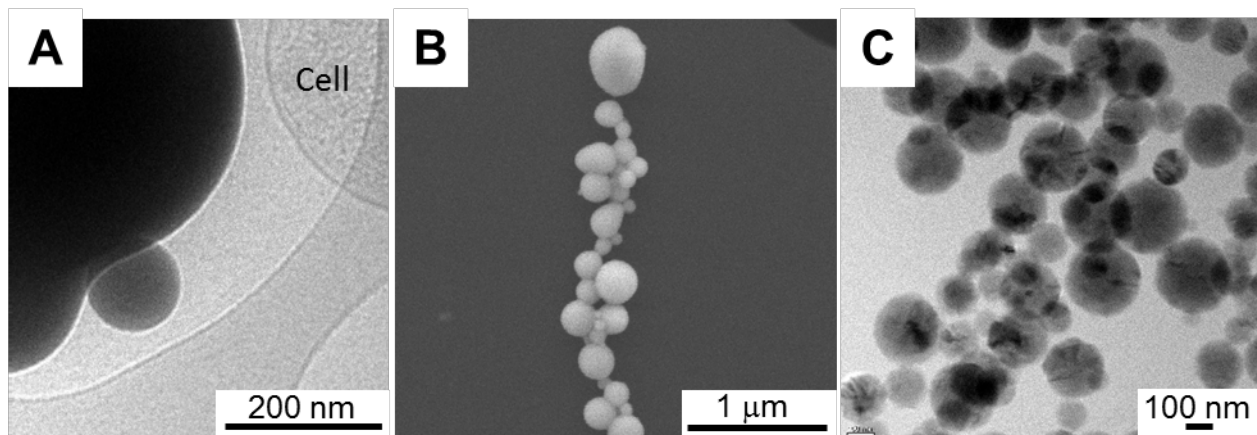
Figure S12. In cultures red CNPs Se^0 (A) coalesce, (B) aggregate and (C) slowly crystallize over time.

Movies S1 and S2: CLSM of field-derived biofilms. Cells were detected by staining their DNA with SYTO BC (Invitrogen product #S34855). **S1**) 3D confocal movie showing several "haystacks" of cells. The biofilm ranges in thickness from 2-12 μm. Scale bar is 5μm. **S2**) 2D Z-slice movie of the same biofilm region. Cells range in length from 0.75 to 2.7 μm. Scale bar is 3μm.

Table S1. Content of growth media employed in this study

Bicarbonate medium	
Ingredient	g/L
NH_4Cl	0.25
NaH_2PO_4	0.6
KCl	0.1
$NaHCO_3$	2.5
vitamins	10 ml
minerals	10 ml
RAGW medium	
Ingredient	g/L
$NaHCO_3$	0.647
KCl	0.030
$MgSO_4.7H_2O$	0.986
$CaSO_4$	0.655
NaCl	0.152
NH_4Cl	0.125

Table S2. List of selenium standard compounds used in valence plot and LSQ linear combination fitting analyses.

Compound	Formula	Temperature/ Source	Crystal system
Organic			
Seleno-diglutathione	$C_{20}H_{32}N_6O_{12}S_2Se$	RT, Freeman 2006[14]	
Seleno-cystathionine	$C_7H_{14}N_2O_4Se$	RT, Freeman 2006[14]	
γ-glutamyl-methyl-seleno-cysteine	$C_9H_{16}N_2O_5Se$	RT, Freeman 2006[14]	
Se-Methyl-seleno-cysteine	$C_4H_9NO_2Se$	RT, Freeman 2006[14]	
Se-ethionine	$C_6H_{13}NO_2Se$	RT, Ryser 2005[15]	
Seleno-DL-cystine*	$C_6H_{12}N_2O_4Se_2$	98K, SA CAS # 2897-21-4*	
		RT, Freeman 2006[14]	
		RT, Ryser 2005[15]	
Seleno-DL-methionine*	$C_5H_{11}NO_2Se$	98K, SA CAS # 1464-42-2*	
		RT, Ryser 2005[15]	
Se-(Methyl)seleno-cysteine hydrochloride*	$C_4H_9NO_2Se \cdot HCl$	98K, SA CAS # 863394-07-4*	
Se(-II)			
Berzelianite	$Cu_{1.8}Se$	RT, Ryser 2005[15]	Cubic
Copper selenide	CuSe	RT, Ryser 2005[15]	N.D.
Zinc selenide	ZnSe	RT, Ryser 2005[15]	Cubic
Se (-I)			
Krutaite	$CuSe_2$	RT, Ryser 2005[15]	Cubic
Penroseite	$(Ni,Co,Cu)Se_2$	RT, Ryser 2005[15]	Cubic
Se (0)			
Red Se from selenate	Se	RT, Microbial, Strawn[γ]	N.D.
Red Se from selenite	Se	RT, Microbial, Ryser 2005[15]	Monoclinic
Red Se 193 nm	Se	RT and 98K, Synthetic	Amorphous
Red Se from selenite*	Se	RT and 98K, microbial*	Amorphous
Grey Se*	Se	RT and 98K, synthetic*	Trigonal
Se foil	Se	RT and 98K, Exafs Materials	Trigonal
Selenium shot 2-6 mm, 99.999%	Se	RT and 98K, AA CAS # 7782-49-2	Amorphous
Selenium black 99+	Se	RT, EMD Millipore # 034-001-00-2	Trigonal
Se (IV)			
Chalcomenite	$CuSeO_3H_2O$	RT, Ryser 2005[15]	Orthorhombic
Mandarinoite	$Fe^{3+}_2Se_3O_9 \bullet 6(H_2O)$	RT, Ryser 2005[15]	Monoclinic
Sodium selenite*	Na_2SeO_3	98K, SA CAS # 10102-18-8*	Tetragonal
		RT, Freeman 2006[14]	
		RT, Ryser 2005[15]	
Calcium selenite	$Ca.H_2O_3Se$	98K, P&B CAS # 13780-18-2	Monoclinic
Copper(II) selenite hydrate	$CuO_3Se \bullet xH_2O$	98K, AA CAS # 10214-40-1	Orthorhombic

Zinc selenite	$ZnSeO_3$	98K, AA CAS # 13597-46-1	Orthorhombic
Se dioxide	SeO_2	98K, SA CAS # 7446-08-4	Trigonal
Selenium tetrachloride	$SeCl_4$	RT, SA CAS # 10026-03-6	Monoclinic

Se(VI)

Calcium selenate	$CaSeO_4$	RT, MP Bio CAS # 14019-91-1	Monoclinic
Sodium selenate*	Na_2SeO_4	98K, SA CAS # 13410-01-0*	Orthorhombic
		RT, Freeman 2006[14]	
		RT, Ryser 2005[15]	
Barium selenate	$BaSeO_4$	98K, AA CAS # 7787-41-9	Orthorhombic
Potassium selenate	K_2SeO_4	98K, AA CAS # 7790-59-2	Orthorhombic
Zinc selenate pentahydrate	$ZnSeO_4 \cdot 5H_2O$	98K, AA CAS # 13597-54-1	Triclinic
Cupric selenate	$H_{10}O_9CuSe$	RT, MP Bio CAS # 10031-45-5	Triclinic
Neodymium selenate	$O_{12}Se_3Nd_2$	98K, MP Bio 05227729	N.D.
Magnesium selenate	O_4MgSe	98K, MP Bio CAS # 14986-91-5	Monoclinic

N.D.= not determined; RT= room temperature; [Y]unpublished, SA= Sigma-Aldrich, AA= Alfa Aesar, P&B= Pfaltz & Bauer.*Standards also measured on STXM at room temperature.

Table S3. Summary of results of LSQ linear combination fitting of XANES spectra on field-derived biofilms and enrichment cultures. Standards compounds employed are listed in Table S2.

Sample	Grey hex. Se	Red am. Se	Selenite	Selenate	Org. Se	Other
Biofilm CG02 (n=29)	ND	96.6	3.4	ND	ND	ND
Culture GWA (n=23)	ND	42.5	35.8	4.3	8.7	8.7
Culture Bicarb (n=18)	5.6	48.5	34.7	5.6	ND	5.6

ND= not detected, n= number of spots measured.

Table S4. EXAFS fitting parameters (see **Figure 6**). k^2-weighted spectra were fitted in q space, in the k range 2-12 Å^{-1}, using a Kaiser-Bessel window. R range used was 1.4-2.5 Å.

Sample	Shell	N	S_0^2	σ^2 (Å^2)	ΔE_0 (eV)	R (Å)
19d bicarb*	Se-Se	2.00	1.011 ± 0.067	0.00282 ± 0.0004	-2.446 ± 0.898	2.33897 ± 0.0034
Biofilm CG02	Se-Se	2.00	1.121 ± 0.068	0.00322 ± 0.0004	-2.440 ± 0.817	2.35510 ± 0.0032

Note: *19-day-old enrichment culture in bicarbonate medium. σ^2 = mean-square disorder of neighbor distance, R = distance to neighboring atom, N = coordination number of neighboring atom, ΔE_0 = shift in threshold energy E_0, S_0^2 = amplitude reduction term.

References

1.   Comolli, L. R.; Duarte, R.; Baum, D.; Luef, B.; Downing, K. H.; Larson, D. M.; Csencsits, R.; Banfield, J. F., A portable cryo-plunger for on-site intact cryogenic microscopy sample preparation in natural environments. *Micros. Res Tech.* **2012,** *75*, (6), 829-836.

2.   Marcus, M. A.; Westphal, A. J.; Fakra, S. C., Classification of Fe-bearing species from K-edge XANES data using two-parameter correlation plots. *J Synch. Rad.* **2008,** *15*, (Pt 5), 463-8.

3.   Hammersley, A. P.; Svensson, S. O.; Hanfland, M.; Fitch, A. N.; Hausermann, D., Two-dimensional detector software: From real detector to idealised image or two-theta scan. *High Press. Res.* **1996,** *14*, (4-6), 235-248.

4.   Nawrocki, E. P. Structural rna homology search and alignment using covariance models. Washington University, 2009.

5.   Quast, C.; Pruesse, E.; Yilmaz, P.; Gerken, J.; Schweer, T.; Yarza, P.; Peplies, J.; Glöckner, F. O., The SILVA ribosomal RNA gene database project: improved data processing and web-based tools. *Nucl. Ac. Res.* **2013,** *41*, (D1), D590-D596.

6.   Stamatakis, A., RAxML Version 8: A tool for Phylogenetic Analysis and Post-Analysis of Large Phylogenies. *Bioinformatics* **2014**.

7.   Saitou, N.; Nei, M., The neighbor-joining method: a new method for reconstructing phylogenetic trees. *Molec. biol. evol.* **1987,** *4*, (4), 406-25.

8.   Kilcoyne, A. L.; Tyliszczak, T.; Steele, W. F.; Fakra, S.; Hitchcock, P.; Franck, K.; Anderson, E.; Harteneck, B.; Rightor, E. G.; Mitchell, G. E.; Hitchcock, A. P.; Yang, L.; Warwick, T.; Ade, H., Interferometer-controlled scanning transmission X-ray microscopes at the Advanced Light Source. *J Synch. Rad.* **2003,** *10*, (Pt 2), 125-36.

9.   Stöhr, J., NEXAFS Spectroscopy. **1992**.

10.   Kirz, J.; Jacobsen, C.; Howells, M., Soft X-ray microscopes and their biological applications. *Quart. rev. biophysics* **1995,** *28*, (1), 33-130.

11.   Pereiro, E.; Nicolas, J.; Ferrer, S.; Howells, M. R., A soft X-ray beamline for transmission X-ray microscopy at ALBA. *J Synch. Rad.* **2009,** *16*, (Pt 4), 505-12.

12.   Fayard, B.; Salomé, M.; Takemoto, K.; Kihara, H.; Susini, J., Some practical considerations about the effects of radiation damage on hydrated cells imaged by X-ray fluorescence microscopy. *J. Elect. Spect. Rel. Phenom.* **2009,** *170*, (1–3), 19-24.

13.   Bao, C.; Wu, H.; Li, L.; Newcomer, D.; Long, P. E.; Williams, K. H., Uranium Bioreduction Rates across Scales: Biogeochemical Hot Moments and Hot Spots during a Biostimulation Experiment at Rifle, Colorado. *Environ. Sci & Technol.* **2014,** *48*, (17), 10116-10127.

14.   Freeman, J. L.; Zhang, L. H.; Marcus, M. A.; Fakra, S.; McGrath, S. P.; Pilon-Smits, E. A. H., Spatial Imaging, Speciation, and Quantification of Selenium in the Hyperaccumulator Plants Astragalus bisulcatus and Stanleya pinnata. *Plant Physiol.* **2006,** *142*, (1), 124-134.

15.   Ryser, A.; Strawn, D.; Marcus, M.; Johnson-Maynard, J.; Gunter, M.; Moller, G., Micro-spectroscopic investigation of selenium-bearing minerals from the Western US Phosphate Resource Area. *Geochem. Trans.* **2005,** *6*, (1), 1.